The Korean Journal of Rheology,
Vol. 5, No. 2, December 1993 pp.109-124

〈연구논문〉

단섬유보강 플라스틱재료의 사출성형 충전공정 수치해석

정성택 · 권태헌

포항공과대학 기계공학과
(1993년 7월 1일 접수)

Numerical Simulation of Injection Molding Filling Process of Short-Fiber-Reinforced Thermoplastics

S. T. Chung and T. H. Kwon

Department of Mechanical Engineering, Pohang Institute of Science and Technology, P.O. Box 125, Pohong 790-600, Korea
(Received July 1, 1993)

요 약

본 연구의 목표는 임의의 3차원 사출성형 금형 공간내에서 단섬유 강화 플라스틱의 충전 공정에서의 과도기적 섬유 방향성을 예측하는 수치 해석 프로그램의 개발에 있다. Hele-Shaw 방정식에 단섬유에 의해서 추가된 응력을 고려한 Dinh-Armstrong의 모델을 도입함으로써 새로운 충전 과정의 압력 지배 방정식이 유도되었다. 새로운 압력 지배 방정식은 단섬유에 의한 응력 때문에 몇개의 새로운 항들을 포함하고 있다. 충전 과정의 해석은 새로운 압력 지배 방정식과 에너지 방정식을 유한 요소법과 유한 차분법을 이용하여 풀고 동시에 배향 텐서(orientation tensor)의 변화 방정식을 4차 Runge-Kutta 방법을 이용하여 풀었다. 단섬유 배향 텐서를 텐서의 변환 법칙을 이용하여 임의의 3차원 금형 공간내의 모든 유한 요소의 중심에서 두께 방향의 모든 유한 차분 격자를 따라 계산하였다. 이러한 방법으로 임의의 3차원 사출 성형 금형 공간내에서 비등온 충전 유동과 과도기적 3차원 섬유 배향 상태를 서로의 상호작용을 고려하여 수치 모사하여 다양한 유동 형태에 따른 단섬유 배향 상태의 변화에 대하여 알아보고자 한다.

Abstract—The present study aims at the development of a numerical simulation program to predict a transient behavior of fiber orientations together with the mold filling simulation for short-fiber-reinforced thermoplastics in arbitrary three-dimensional injection mold cavities. Dinh-Armstrong model including an additional stress due to the existence of fibers is incorporated into the Hele-Shaw equation to result in a new pressure equation governing the filling process. The mold filling simulation is performed by solving the new pressure equation and energy equation via a finite element/finite difference method as well as evolution equations for the second-order orientation tensor via the fourth-order Runge-Kutta method. The fiber orientation tensor is determined at every layer of each element across the thickness of molded parts with appropriate tensor transformations for arbitrary three-dimensional cavity space.

Keywords: Fiber orientation, injection molding, filling process, short-fiber-reinforced thermoplastics, numerical analysis

1. Introduction

In injection molding of short-fiber-reinforced thermoplastics, the prediction of fiber orientation is very improtant to obtain the desired mechanical properties of injection molded parts. It is well known that anisotropic mechanical properties are significantly affected by the final fiber orientation state. The flow during a mold filling process plays an important role in forming a flow-induced fiber orientation field. However, the flow field is also affected by the orientation of fibers. Therefore a mold filling simulation of fiber-filled polymer must include an anisotropic constitutive equation in order to describe the system completely.

Jeffery's model [1], which was developed for the motion of a single ellipsoidal particle immersed in a viscous fluid, has been a basis of most studies in this field. Since this model does not account for the fiber-fiber interaction and does not consider the effect of fiber orientation on the velocity field, this is only valid for sufficiently dilute suspension. Givler *et al.* [2], calculated fiber orientations from the numerical integration of Jeffery's equation along streamlines via the finite element method. Folgar and Tucker [3] developed a model for the orientation behavior of concentrated suspensions by adding a diffusion term to the Jeffery's equations in order to account for fiber-fiber interactions. Dinh and Armstrong [4] developed a rheological equation of state for semiconcentrated suspensions. They replaced the multiparticle problem with a single-particle one with the subsequent use of Batchelor's cell model [5] to estimate the drag on a test fiber to account approximately for fiber-fiber interactions. Bibbo *et al.* [6], showed a good agreement between computed and measured rheological properties using Dinh and Armstrong model. In recent years several different methods have been used to describe the fiber orientation states. Advani and Tucker [7] developed the use of tensors to describe and predict fiber orientation. These tensors offer a concise representation of orientation state but a closure approximation is required to obtain a closed set of evolution equations for orientation tensors. Altan *et al.* [8], studied tensorial approximations for the description of orientation state for fiber suspensions in homogeneous flows. A closure approximation for three-dimensional structure tensors was proposed by Advani and Tucker [9] modifying the scalar measure of fiber alignment. Recently, Advani and Tucker [10] developed a numerical method to predict the orientation of fibers in a thin, flat part. They combined a finite element/control volume method of the mold filling flow and a finite element calculation for the transient orientation problem. But their orientation calculation was limited to flat parts. Altan *et al.* [11], presented a numerical method to predict the transient three-dimensional fiber orientations in Hele-Shaw flows in irregularly shaped planar cavities. Each fiber location was traced during mold filling and along these paths the independent components of fourth order orientation tensors were solved at zero volume fraction limit. Frahan *et al.* [12], developed a numerical method for calculating fiber orientation in the midsurface of a molded part of small thickness in injection molding. Two-dimensional fiber orientation was predicted in three-dimensional geometries in the absence of coupling between the flow calculation and the fiber orientation. More recently, many researchers simulated the short fiber orientation in an extrudate swell, an injection molding and a fountain flow field [13-16].

This paper presents a numerical simulation that couples a non-isothermal mold filling flow and a transient three-dimensional fiber orientation in arbitrary three-dimensional thin cavities in injection molding. The first section reviews the theory describing the fiber orientation states and the equation of change for the orientation tensors. Then presented is a modeling of the coupled mold filling process with Dinh and Armostrong's rheological equation of state for semiconcentrated fiber suspensions. The numerical analysis describes the development of a computer simulation program to predict the mold filling flow field modified by the presence of fibers and the flow induced fiber

orientation states. The program combines finite element/finite difference methods for mold filling simulation with a numerical method for an integration of the evolution equations for the fiber orientation tensor. Finally, several numerical results are presented.

2. Governing Equations

2.1. Fiber Orientation

There are several different approaches to describe the fiber orientation. The simplest form is the scalar angle between the fiber and one of the reference axes. In any injection molded parts there are fibers oriented in many different directions. A single orientation angle cannot describe the true orientation state of fibers. The most complete, but complex way to describe the orientation state is the use of a probability distribution function, ψ, which is associated with a unit vector $\mathbf{p}$ along the axis of the fiber indicating the orientation. The distribution function, $\psi(\mathbf{p}, t)$, is defined such that it gives the probability of a fiber having an alignment in the direction $\mathbf{p}$. The probability distribution function must be periodic, normalized and satisfy the continuity condition [7]. Using the distribution function to calculate the fiber orientation state everywhere in the part would make the calculation too long and expensive for a practical use. A more compact representation of fiber orientation state is thus needed.

Advani and Tucker [7] showed the use of even order tensors as a more concise description for the orientation state in a suspension or composite system. The second- and fourth-order orientation tensors are

$$a_{ij}=\oint p_i p_j \psi(\mathbf{p}, t)\, d\mathbf{p}$$

$$a_{ijkl}=\oint p_i p_j p_k p_l \psi(\mathbf{p}, t)\, d\mathbf{p} \qquad (1)$$

The second- and fourth-order orientation tensors are completely symmetric and the trace of a_{ij} is unity, which is the normalization condition. An advantage of using orientation tensors is computational efficiency. We will use the second-order three-dimensional orientation tensor to descirbe the three-dimensional orientation state. In this case there are only five independent tensor components.

To predict the flow-induced orientation state by using compact orientation tensors, we need the equation of change (i.e. evolution equation) for orientation tensors. One takes the material derivative of Eq. (1) with the help of Jeffery's equation and continuity equation for ψ, then obtains the equations of change for orientation tensors [7].

In practical injection molded parts of short-fiber-reinforced thermoplastics, there are too many fibers to consider the fluid as dilute suspensions, so Jeffery's equation becomes invalid. The orientation state of concentrated suspensions is similar to that of dilute suspensions. Howevers, as the volume fraction of fibers increases, the orientation state is influenced by fiber-fiber interactions. It is very difficult to model physically the fiber-fiber interactions. So Folgar and Tucker [3] suggested a phenomenological model. They added a diffusive type of term to Jeffery's equation by introducing a pheomenolgical coefficient for modeling the randomizing effect of mechanical interactions between fibers.

Folgar and Tucker's equation [7] of change for the second-order orientation tensor in a concentrated suspension is

$$\frac{Da_{ij}}{Dt}=-\frac{1}{2}(\omega_{ik}a_{kj}-a_{ik}\omega_{kj})+\frac{1}{2}\lambda(\dot{\gamma}_{ik}a_{kj}+a_{ik}\dot{\gamma}_{kj}-2\dot{\gamma}_{kl}a_{ijkl})+2C_I\dot{\gamma}(\delta_{ij}-\alpha a_{ij}) \qquad (2)$$

where δ_{ij} is a unit tensor and α equals 3 for three-dimensional orientation. ω_{ij} and $\dot{\gamma}_{ij}$ are the vorticity and the rate of deformation tensors, respectively, defined in terms of velocity gradients as

$$\omega_{ij}=\frac{\partial u_j}{\partial x_i}-\frac{\partial u_i}{\partial x_j}, \quad \dot{\gamma}_{ij}=\frac{\partial u_j}{\partial x_i}+\frac{\partial u_i}{\partial x_j}$$

$\dot{\gamma}$ is the generalized shear rate defined by

$$\dot{\gamma}=\sqrt{\frac{1}{2}\dot{\gamma}_{ij}\dot{\gamma}_{ji}}$$

And λ is a parameter related to the particle shape. It is given as

$$\lambda=\frac{r_e^2-1}{r_e^2+1}$$

where r_e is the aspect ratio of the fiber. The dimensionless interaction coefficient C_I describes the strength of fiber-fiber interactions. In fact, C_I could be variable depending on the fiber orientation state, fiber aspect ratio, fiber volume fraction, etc. Without a detailed model of interactions there is no way to predict C_I; it is assumed to be constant in the present study.

To solve Eq. (2) in terms of a_{ij} we must introduce a suitable closure approximation for the fourth-order tensor a_{ijkl}. There are several types of closure approximations: the linear closure approximation is better for a random distribution of orientation, while the quadratic closure approximation is exact for a perfectly aligned orientation state. A hybrid closure approximation, which mixes the linear and quadratic forms according to a scalar measure of orietation f, performed best for a wider range of orientation states [9]. We will use the hybrid closure approximation given for the three-dimensional orientation in [9].

$$a_{ijkl}=(1-f)\hat{a}_{ijkl}+f\tilde{a}_{ijkl} \tag{3}$$

where $\hat{a}_{ijkl}$ and $\tilde{a}_{ijkl}$ denote the linear closure approximation and the quadratic closure approximation, respectively. The scalar measure of orientation for three-dimensional orientation field is defined by

$$f=1-27\ \det[a_{ij}]$$

f varies from zero (in case of a random orientation) to unity (in case of a perfectly aligned orientation), so that f can be regarded as a measure of orientation.

2.2. Injection Molding Filling Flow

In injection molding filling flow of short-fiber-reinforced thermoplastics, there exists the coupling between the flow field and the fiber orientation. Several models are available for calculating flows coupled with fiber orientation. Dinh and Armstrong [4] developed a rheological equation of state for semiconcentrated fiber suspensions. Their model treats slender cylindrical fibers and ignores the fiber thickness effect. The model is valid for a semiconcentrated region where the average spacing between neighboring fibers is greater than its diameter D but less than its length L. Within this concentration range, fiber-fiber interactions are taken into account by utilizing a self-consistent cell model and considering a representative fiber immersed in an effective medium. The constitutive equation of this model can be described as follows

$$\tau_{ij}=\eta(u_{i,j}+u_{j,i})+\eta\frac{\pi n L^3}{6\ \ln(2h/D)}u_{k,l}a_{ijkl} \tag{4}$$

$$h=\begin{cases}(nL)^{-1/2} & \text{(aligned)}\\ (nL^2)^{-1} & \text{(random)}\end{cases}$$

where

τ_{ij} = total stress tensor
η = viscosity of the thermoplastic medium
$u_{i,j}=\partial u_i/\partial x_j$: velocity gradient tensor
n = number of fibers per unit volume
h = average distance from a given fiber to its nearest neighbors

In the present simulation, it is assumed that the average distance from a given fiber to its nearest neighbors, h, is linear in terms of the scalar measure of orientation f. When the number of fibers per unit volume n is greater than $1/(DL^2)$, the average distance between fibers is assumed to be the same as $h_{aligned}$ for the aligned orientation state. That is,

$$h=(1-f)\ h_{random}+f\,h_{aligned}\quad \text{for}\quad \frac{1}{L^3}<n\le\frac{1}{DL^2}$$

$$h=h_{aligned}\quad \text{for}\quad \frac{1}{DL^2}<n<\frac{1}{D^2L} \tag{5}$$

The thickness of injection molded parts is usually much smaller than other characteristic dimensions of the part. So, the injection molding filling flow can be approximated by the use of the lubrication approximation, based upon the fact that the

velocity gradients in the thickness are much larger than those in the in-plane directions. One then obtains the Hele-Shaw approxmination of the viscous flow [17]. A fountain flow is observed at the flow front where the flow field is fully three-dimensional. However, it is known that the size of this region is of the order of a few gap widths and thus the fountain flow effect is neglected in the present study. The flow of fiber suspensions in narrow gaps was extensively investigated by Tucker [19]. When the gap is very thin but interaction (or diffusion) effects between fibers introduce some slight out-of-plane orientation, the gapwise shear stress term still dominates the momentum balance. Also, pressure p is still independent of gapwise coordinates z. Thus, the essence of the lubrication approximation is retained. The appropriate simplification of the constitutive equation in such a case is

$$\tau_{3\alpha}=\eta u_{\alpha,3}+\eta\frac{\pi n L^3}{6\ \ln(2h/D)}(u_{1,3}a_{3\alpha 13}+u_{2,3}a_{3\alpha 23}) \quad (6)$$

where, α takes the value 1 and 2. The coordinate system in Eq. (6) is chosen such that 3 is along the thickness direction, 1 and 2 lying on the plane, as indicated in Fig. 1.

Under the above simplification, the injection molding filling flow for non-dilute fiber suspensions is governed by the momentum equation

$$0=-\frac{\partial p}{\partial x}+\frac{\partial}{\partial z}\left[\eta\frac{\partial u}{\partial z}+\eta N\left(\frac{\partial u}{\partial z}a_{3113}+\frac{\partial v}{\partial z}a_{3123}\right)\right]$$
$$0=-\frac{\partial p}{\partial y}+\frac{\partial}{\partial z}\left[\eta\frac{\partial v}{\partial z}+\eta N\left(\frac{\partial u}{\partial z}a_{3213}+\frac{\partial v}{\partial z}a_{3223}\right)\right] \quad (7)$$

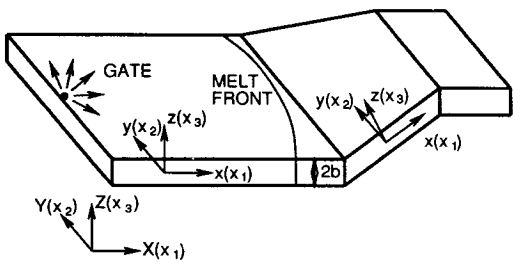

Fig. 1. Schematic diagram of a cavity with coordiate system.

where

$$N\equiv\frac{\pi n L^3}{6\ \ln(2h/D)}$$

and by the mass conservation equation

$$\frac{\partial}{\partial x}(\bar{bu})+\frac{\partial}{\partial y}(\bar{bv})=0 \quad (8)$$

where b is the half gap thickness of the part, which may be a function of x and y. "$-$" denotes an average over z, the gapwise coordinate. And η, a function of shear rate and temperature T, is the viscosity of the thermoplastic medium. In the present study, a modified cross model has been employed as follows

$$\eta(\dot{\gamma},T)=\frac{\eta_o}{1+C(\eta_o\dot{\gamma})^{1-n}},\quad \eta_o=B\ \exp\left(\frac{T_b}{T}\right) \quad (9)$$

where n, B, C and T_b are constants for a given material and η_o is zero-shear-rate viscosity. Appropriate boundary conditions in the z-direction are given by

$$\begin{aligned} &u=0 \qquad v=0 \qquad \text{at } z=b\\ &\partial u/\partial z=0 \quad \partial v/\partial z=0 \quad \text{at } z=0 \end{aligned} \quad (10)$$

Integration of Eq. (7) with the help of Eq. (10) results in

$$\begin{aligned} \frac{\partial u}{\partial z}&=\frac{\partial p}{\partial x}\frac{z}{\eta}-N^x\frac{\partial p}{\partial x}\frac{z}{\eta}-N^{xy}\frac{\partial p}{\partial y}\frac{z}{\eta}\\ \frac{\partial v}{\partial z}&=\frac{\partial p}{\partial y}\frac{z}{\eta}-N^y\frac{\partial p}{\partial y}\frac{z}{\eta}-N^{xy}\frac{\partial p}{\partial x}\frac{z}{\eta} \end{aligned} \quad (11)$$

$$u=-\frac{\partial p}{\partial x}\int_z^b\frac{\tilde{z}}{\eta}d\tilde{z}+\frac{\partial p}{\partial x}\int_z^b N^x\frac{\tilde{z}}{\eta}d\tilde{z}+\frac{\partial p}{\partial y}\int_z^b N^{xy}\frac{\tilde{z}}{\eta}d\tilde{z}$$
$$v=-\frac{\partial p}{\partial y}\int_z^b\frac{\tilde{z}}{\eta}d\tilde{z}+\frac{\partial p}{\partial y}\int_z^b N^y\frac{\tilde{z}}{\eta}d\tilde{z}+\frac{\partial p}{\partial x}\int_z^b N^{xy}\frac{\tilde{z}}{\eta}d\tilde{z} \quad (12)$$

where

$$N^x\equiv\frac{Na_{3113}(1+Na_{3223})-N^2a_{3123}a_{3213}}{(1+Na_{3113})(1+Na_{3223})-N^2a_{3123}a_{3213}}$$
$$N^y\equiv\frac{Na_{3223}(1+Na_{3113})-N^2a_{3123}a_{3213}}{(1+Na_{3113})(1+Na_{3223})-N^2a_{3123}a_{3213}}$$
$$N^{xy}\equiv\frac{Na_{3123}}{(1+Na_{3113})(1+Na_{3223})-N^2a_{3123}a_{3213}} \quad (13)$$

The two last terms in Eq. (12) indicate the coupling effect of the pressure gradient to the velocity in x and y direction, respectively. It should be noted that the velocity vector is not in the direction of $-\nabla p$, which is different from a fundamental characteristic of Hele-Shaw type flows of thermoplastics without fibers. The gapwise average velocities are obtained by integration of Eq. (12):

$$\bar{u}=-\frac{S}{b}\frac{\partial p}{\partial x}+\frac{S^x}{b}\frac{\partial p}{\partial x}+\frac{S^{xy}}{b}\frac{\partial p}{\partial y}$$
$$\bar{v}=-\frac{S}{b}\frac{\partial p}{\partial y}+\frac{S^y}{b}\frac{\partial p}{\partial y}+\frac{S^{xy}}{b}\frac{\partial p}{\partial x} \quad (14)$$

where

$$S\equiv\int_0^b\frac{\tilde{z}^2}{\eta}d\tilde{z}$$
$$S^x\equiv\int_0^b N^x\frac{\tilde{z}^2}{\eta}d\tilde{z}$$
$$S^y\equiv\int_0^b N^y\frac{\tilde{z}^2}{\eta}d\tilde{z}$$
$$S^{xy}\equiv\int_0^b N^{xy}\frac{\tilde{z}^2}{\eta}d\tilde{z} \quad (15)$$

Hence, substituting Eq. (14) into Eq. (8) gives the pressure equation as follows

$$\frac{\partial}{\partial x}\left[(S-S^x)\frac{\partial p}{\partial x}-S^{xy}\frac{\partial p}{\partial y}\right]+\frac{\partial}{\partial y}\left[(S-S^y)\frac{\partial p}{\partial y}-S^{xy}\frac{\partial p}{\partial x}\right]=0 \quad (16)$$

Boundary conditions on the pressure equation are

$$p=0 \quad \text{on the moving flow front}$$
$$\bar{u}\cdot n_x+\bar{v}\cdot n_y=0 \quad \text{on the impermeable boundaries} \quad (17)$$

In order to deal with the non-isothermal flow, the energy equation is also to be solved during the filling process. In a thin cavity mold, the energy equation can be simplified as

$$\rho C_p\left(\frac{\partial T}{\partial t}+u\frac{\partial T}{\partial x}+v\frac{\partial T}{\partial y}\right)=k\frac{\partial^2 T}{\partial z^2}+\eta\dot{\gamma}^2 \quad (18)$$

Appropriate boundary conditions in the z-direction for the above governing equation are given by

$$T=T_w \quad \text{at } z=b$$
$$\partial T/\partial z=0 \quad \text{at } z=0 \quad (19)$$

3. Numerical Analysis

3.1. Mold Filling Flow

The injection molding filling flow is, in its nature, non-isothermal and non-Newtonian with a moving boundary (the flow front). It is difficult to treat the moving flow front in cavities of complex geometry. Here, a finite element method is used to solve Eq. (16) for the pressure distribution over the flow domain while the gapwise temperature distribution is solved using a finite difference technqiue [17, 18].

In the present treatment, we employ thin shell triangular elements for the cavity and linear shape functions for p. Accordingly, on each element, e, the pressure field is of the form:

$$\tilde{p}^{(e)}=\sum_{j=1}^{3}\Psi_j^{(e)}p_j^{(e)} \quad (20)$$

where j corresponds to the three vertex nodes with Ψ_j being linear interpolation functions and p_j being the nodal pressures. A Galerkin method is employed on Eq. (16) such that the resulting governing equation for any interior node is given by

$$\int_\Omega\left[(S-S^x)\frac{\partial\Psi_i}{\partial x}\frac{\partial\Psi_j}{\partial x}+(S-S^y)\frac{\partial\Psi_i}{\partial y}\frac{\partial\Psi_j}{\partial y}-S^{xy}\frac{\partial\Psi_i}{\partial x}\frac{\partial\Psi_j}{\partial y}-S^{xy}\frac{\partial\Psi_i}{\partial y}\frac{\partial\Psi_j}{\partial x}\right]d\Omega\ p_j=0 \quad (21)$$

The above nonlinear system of euqation can be solved by iteration.

The melt front tracking algorithm with fixed mesh associates a control volume with each node. The nodal fill factor, which is defined as the filled fraction of nodal control volume and varies from zero (empty node) to unity (completely filled node), is assigned to each node. Partially filled nodes, which have the fill factor greater than zero and less than unity, are considered as the melt flow front nodes. Pressure values are calculated at the completely filled nodes by solving the finite

element equations. And the finite difference form is also used to solve Eq. (18) for gapwise temperature distribution in the present study. The flow front is advanced at each filling time step by updating the nodal fill factor according to mass balance between connected nodes. The procedure is repeated until the entire mold is filled. The finite element/finite difference scheme can simulate the mold filling flow with non-isothermal conditions in very complex geometries [17, 18].

3.2. Fiber Orientation

It is well known that gapwise variation in shearing and stretching deformation of fluid produces distinct orientation structure along the gapwise direction. The evolution equation for the second-order orientation tensor, Eq. (2), in three-dimension produces a system of five coupled, non-linear, differential equations. There are many numerical methods to solve these kinds of evolution equations [2, 10, 11, 12]. In the present study these are solved at the centroids of the same finite element mesh as is used for the mold filling analysis, based on its local coordinate system, as shown in Fig. 1. This method is useful because the velocity gradient field is calculated based on the local coordinate system from the filling analysis and the flowability constants in Eq. (5) are determined at the centroid of each element. Therefore, Eq. (2) can be rewritten as follows

$$\frac{\partial a_{ij}}{\partial t}+u\frac{\partial a_{ij}}{\partial x}+v\frac{\partial a_{ij}}{\partial y}=-\frac{1}{2}(\omega_{ik}a_{kj}-a_{ik}\omega_{kj})+\frac{1}{2}\lambda(\dot{\gamma}_{ik}a_{kj}+a_{ik}\dot{\gamma}_{kj}-2\dot{\gamma}_{kl}a_{ijkl})+2C_I\dot{\gamma}(\delta_{ij}-\alpha a_{ij}) \quad (22)$$

Fiber orientation calculations are performed concurrently with the mold filling simulation. The orientation tensor components are calculated at each layer subdividing local part thickness, for each element in the mesh, by a fourth-order Runge-Kutta method for the time integration.

The Eq. (22) requires the velocity gradient at the centroid of element at each layer.

$$u_{i,j}=\begin{bmatrix} u_{,x} & u_{,y} & u_{,z} \\ v_{,x} & v_{,y} & v_{,z} \\ 0 & 0 & 0 \end{bmatrix} \quad (23)$$

However, the filling simulation provides only nodal pressures and shear velocity gradients, $u_{,z}$ and $v_{,z}$, from Eq. (11), at the centroid of element at each layer. In order to evaluate the spatial derivatives of velocity in x and y directions, one needs the nodal velocities. Because the velocity is proprotional to the pressure gradient, one can find the velocities u and v using Eq. (12) at the centroid of element at each layer. Then, nodal velocities are evaluated by a global averaging procedure, i.e. weighted by the associated subvolume of neighboring elements.

The Eq. (22) also requires the spatial gradients of orientation tensor. An *ad hoc* procedure was developed to evaluate the spatial gradients of the orientation tensor in view of the upwinding scheme. In Fig. 2, the directional derivatives of the orientation tensor components, based on the local coordinate system of element (e), between centroids of element (e) and element (e_k) are given by

$$\nabla a_{ij}\cdot\hat{l}_k=\frac{\partial a_{ij}}{\partial l} \quad (24)$$

where $\hat{l}_k$ is a unit vector of a vector $(\Delta x^k\hat{i}+\Delta y^k\hat{j})$, directed from the centroid of element (e) to that of element (e_k), k=1, 2. This is rewritten as follows

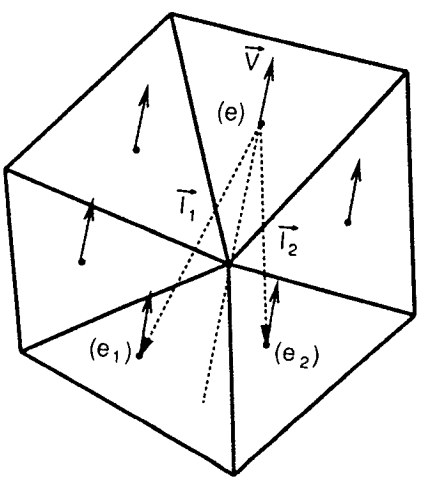

Fig. 2. Treatment of convection term for fiber orientation.

$$\frac{\partial a_{ij}^{(e_k)}}{\partial x}\Delta x^k+\frac{\partial a_{ij}^{(e_k)}}{\partial y}\Delta y^k=a_{ij}^{(e_k)}-a_{ij}^{(e_k)},\ k=1,2 \tag{25}$$

As far as the upwinding scheme is concerned, two elements for k=1 and 2 are chosen from the upwinding direction associated with the element (e), as indicated in Fig. 2. From the above two linear algebraic equations (25), one can find the spatial derivatives of orientation tensor, $\partial a_{ij}/\partial x$ and $\partial a_{ij}/\partial y$. Here one needs the tensor transformation of orientation state of element (e_k) to the local coordinate system of element (e). As a special case, when the plane of element (e) is different from that of element (e_k), it is assumed that the orientation state of fibers is preserved across the folds. The assumption is that the orientation state in the bent plate is the same that of flat plate. For this assumption one needs an additional tensor transformation which rotates the fibers by the angle θ between the folds.

To start the numerical simulation it is needed to specify the initial orientation of fibers at the gates. It may be noted that the fiber orientation at the gate is usually not known. Thus the initial orientation state at the gate may be assigned as either random distribution or aligned distribution in the flow direction. As the melt front advances during mold filling process, more elements will be included in the computational domain. In each time step, elements which include at least one full filled vertex node are considered as new elements to be added for that step. The initial orientation state at the new elements may be obtained by convecting the orientation state from neighboring element which is selected in view of the upwinding scheme. Omitting the convection terms, Eq. (22) is integrated over the time step using the velocity gradients and orientation state of the neighboring element. It provides the orientation of the fiber that has started at the neighboring element at the beginning of the time step and arrived at the new element at the next time step.

The overall numerical scheme for the mold filling flow together with the fiber orientation is schematically summarized in Fig. 3. The computer

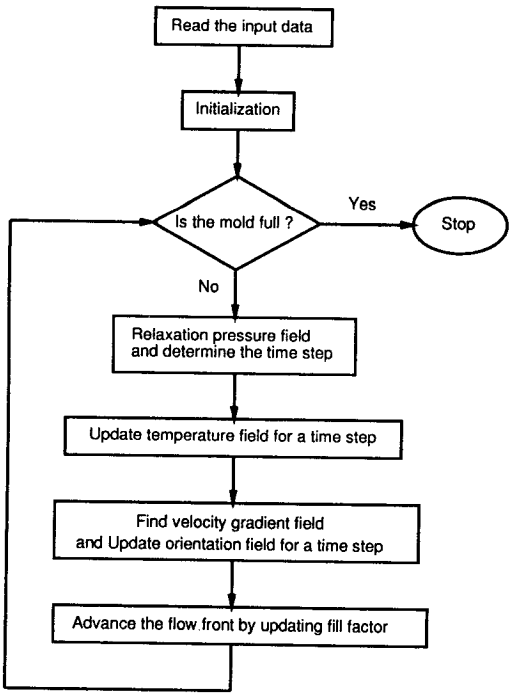

Fig. 3. Overall numerical scheme.

program developed in the present study can calculate the coupled flow field and the flow-induced fiber orientation in the injection molding of arbitrary thin three-dimensional geometries.

4. Results of Numerical Analysis

Numerical results for two different cavity geometries will be discussed in the present section. The thermal properties and polymer melt viscosity of polypropylene used in the following numerical simulations are as follows;

density, $\rho=0.77$ gm/cm^3

specific heat, $C_p=3.46E+07$ erg/(gm K)

thermal conductivity, k=1.51E+04 erg/(sec cm K)

coefficient of viscosity function, n=3.5E-01

coefficient of viscosity function, B=9.6E-02 gm/(cm sec)

coefficient of viscosity function, C=4.8E-04 (gm/(cm sec^2))$^{n-1}$

coefficient of viscosity function, $T_b=5.9E+03$ K

4.1. Numerical Results with a Tension Test Specimen

Numerical simulations have been carried out for a cavity geometry of a tension test specimen with a pin end gate. The dimension of a tension test specimen of ASTM standard is as follows;

length over-all = 18.3 cm
width over-all = 1.9 cm
length of narrow section = 5.7 cm
wideth of narrow section = 0.6 cm
thickness = 0.2 cm

and the input data are as follows;

inlet flow rate, $Q = 5\ cm^3/sec$
inlet melt temperature, $T_m = 200℃$
mold wall temperature, $T_w = 30℃$
the number of fibers per unit volume, $n = 1/mm^3$
length of fiber, $L = 1.0\ mm$
diameter of fiber, $D = 0.04\ mm$
phenomenological coefficient, $C_I = 0.001$

Fig. 4 shows the finite element mesh of tension test specimen, which contains 520 elements, 327 nodes and 14 grid points through the thickness direction. Fig. 5(a) and (b) show the successive flow fronts and the velocity fields, respectively, when the cavity gets filled. One can see the diverging flow around the gate followed by parallel flow, converging-parallel-diverging and parallel flow. Fig. 6 shows the orientation fields at the end of filling at four different layers when a random orientation is imposed at the gate as an initial condition. Three eigenvectors with the magnitude of each eigenvalue of the second-order orientation tensor are plotted to represent the orientation state. Fig. 6(a) is the orientation distribution at the grid point 1, core layer (i.e. the center layer). Here the flow around the gate is extensional and fibers are seen to align in the direction perpendicular to the flow direction. Fig. 6(b) and (c) are the orientation distribution at the grid point 3 and 5, at which the normalized half gap thickness

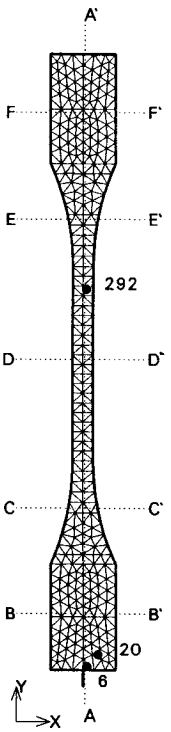

Fig. 4. Finite elment mesh for a tension test specimen with 520 elements and 327 nodes.

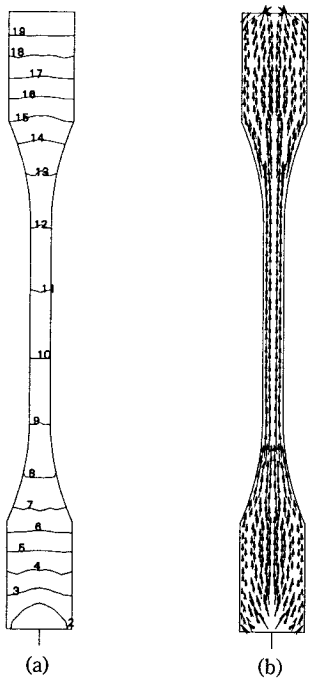

Fig. 5. Filling simulation results for a tension test specimen: (a) filling pattern (step increment = 0.0464 sec, filling time = 0.8807 sec) and (b) velocity field.

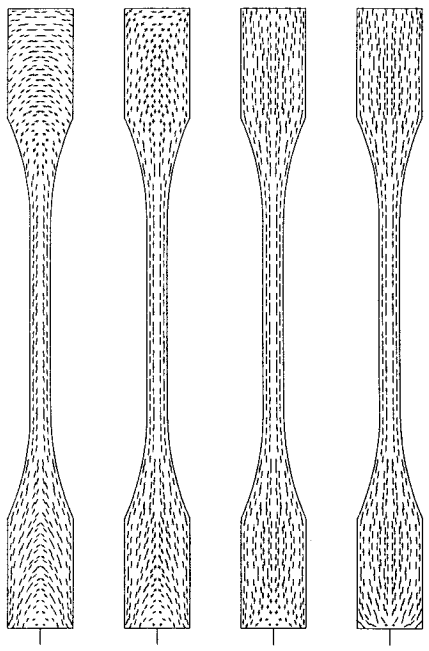

Fig. 6. Fiber orientation state when the cavity is filled for a tension test specimen: (a) at z=0, (b) at z=0.2b, (c) at z=0.4b and (d) at z=0.9 b.

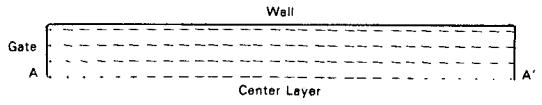

Fig. 7. Longitudinal (on y−z plane) fiber orientation state with a view direction along x-direction for a tension test sepcimen at cross section A−A′ indicated in Fig. 4.

equals to 0.2 and 0.4 respectively. Here the flow involves both shear and extensional effects. Fig. 6 (d) presents the orientation distribution at the grid point 13, skin layer (i.e. surface layer), at which the normalized half gap thickness equals to 0.9. It is clear that shear effects are dominant here with fibers tending to align in the flow direction. Fig. 7 shows the longitudinal fiber orientation state at cross section A−A′ indicated in Fig. 4. Most of the fibers are aligned to the flow direction with a slight inclination toward the center layer.

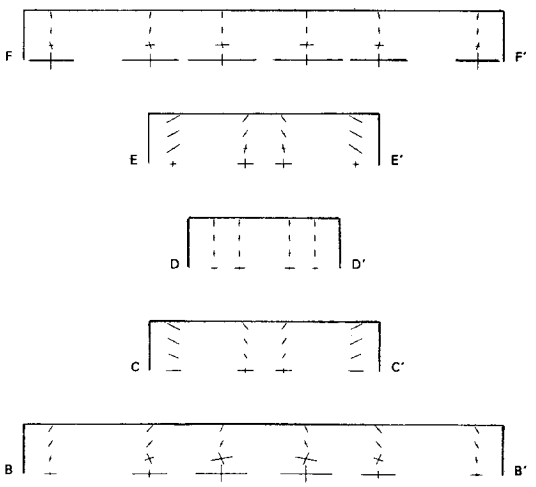

Fig. 8. Transverse (on x−z plane) fiber orientation state with a view direction along y-direction for a tension testk specimen at cross section B−B′, C−C′, D−D′, E−E′ and F−F′ indicated in Fig. 4.

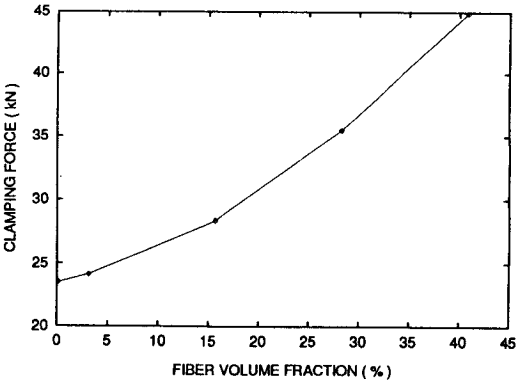

Fig. 9. Clamping force versus fiber volume fraction with a constant inlet flow rate, 5 cm^3/sec, for a tension test specimen.

Fig. 8 shows the transverse fiber orientation state at several cross sections indicated in Fig. 4. Here, one can see the complex fiber orientation state. But at converging flow region, cross section C−C′, fibers are inclined to the inward. While at diverging flow region, cross section E−E′, fibers are inclined to the outward.

4.1.1. Effect of the Concentration of Fibers

Fig. 9 shows the effect of fiber volume fraction

on the clamping force. This effect results from the calculation of the coupled flow field in the present study. One can find that the clamping force increases asymptotically as the number of fibers increases as expected. In this particular case, when the fiber volume fraction is greater than 3.1%, n becmes larger than $1/(DL^2)$ so that the average distance between fibers for aligned orientation state, $h_{aligned}$, is used for h, as explained in Eq. (5). It may just be mentioned that most of fibers are found to be aligned to the flow direction except near the gate according to numerical analysis results. Therfore, this *ad hoc* treatment for determining h seems to be acceptable.

Fig. 10 shows the variation of the velocity components u and v across the gapwise direction at two different elements for two cases of fiber volume fractions. At the element 6 at which the random initial orientation state is imposed at every layer, the difference of the magnitude of x and y directional velocity components decreases as the volume fraction increases. This tendency might be explained by the fact that the coupling effect as indicated in Eq. (12) becomes stronger as the number of fibers per unit volume n, thus N increases. At the element 20 near the gate, the velocity profile tends to be flattened as the volume fraction increases. It may be just mentioned that, in the narrow section of the tension test specimen, the velocity profile remains almost unchanged with the volume fraction. The out-of-plane component of the fiber orientation tensor a_{ij} in the narrow region is almost zero at every layer (see Fig. 7), resulting in insignificant effect of fibers on the velocity field according to Eqs. (12) and (13).

Fig. 11 shows the variation of the temperature across the gapwise direction at the element 20. One can find that the volume fraction of fibers has little effect on the variation of temperature.

4.1.2. Effect of the fiber-fiber interaction coefficient C_I

The dimensionless coefficient C_I describes the strength of the randomizing effect of mechanical interaction between fibers. Fig. 12 shows the fiber orientation state for $C_I=0.05$ which should be compared with Fig. 6 for $C_I=0.001$. It is clear that

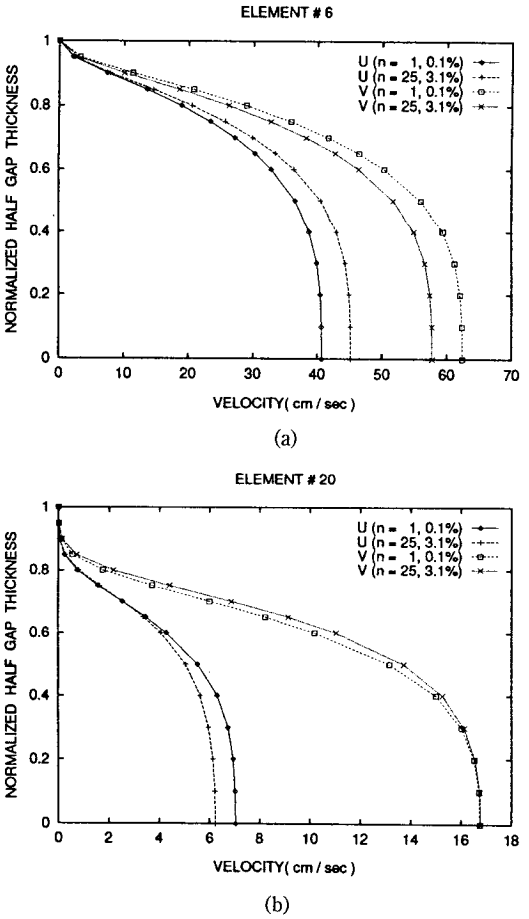

Fig. 10. Variation of velocity components along the gapwise direction for a tension test specimen: (a) at element 6 and (b) at element 20 indicated in Fig. 4.

the fiber orientation state approaches to the randomized orientation state, as the magnitude of C_I increases. The flow field is also affected by the magnitude of C_I. Fig. 13 shows the effect of C_I on the clamping force with the fiber volume fraction n=3.1% fixed. It is found that the clamping force increases as the magnitude of C_I increases because the extra stress term increases as the fiber orientation becomes more randomized.

In case of the phenomenological coefficient C_I being zero, a stable orientation state is observed near the center layer and is found to be almost the same as those in Fig. 6 with $C_I=0.001$. But near the surface layer one can observe an unsta-

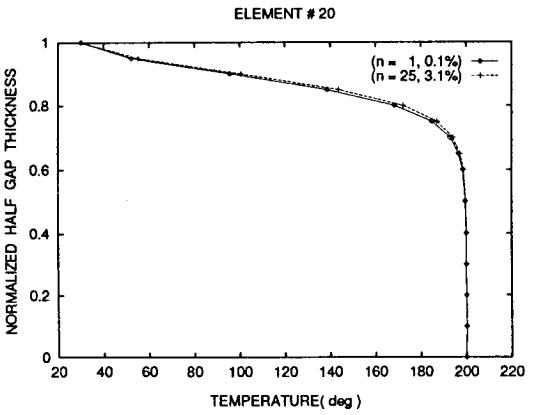

Fig. 11. Variation of temperature along the gapwise direction for a tension test specimen at element 20 indicated in Fig. 4.

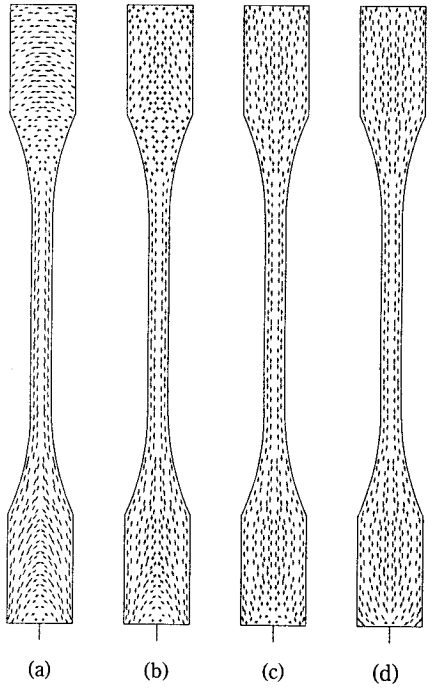

Fig. 12. Fiber orientation state with $C_I=0.05$ when the cavity is filled for a tension test specimen: (a) at $z=0$, (b) at $z=0.2b$, (c) at $z=0.4$ b and (d) at $z=0.9b$.

ble oscillatory oirentation state. For instance, Fig. 14(a) shows the transient behavior of orientation tensor component in case of C_I being zero at the

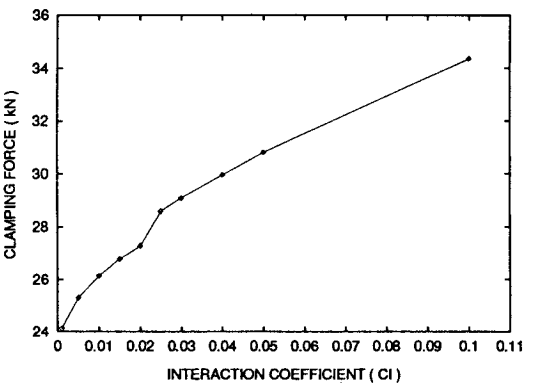

Fig. 13. Clamping force versus fiber-fiber interaction coefficient C_I with the fiber volume fraction n=3.1% fixed and a constant inlet flow rate, 5 cm^3/sec, for a tension test specimen.

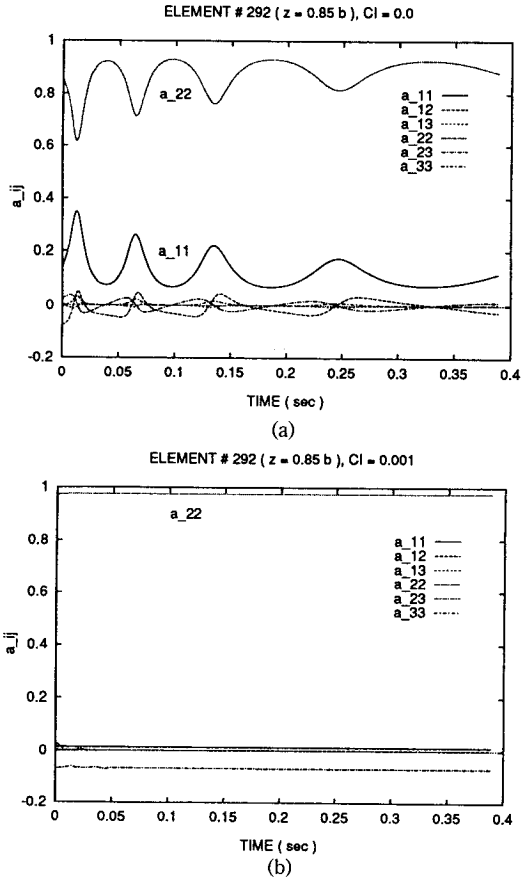

Fig. 14. Effect of the dimensionless fiber-fiber interaction coefficient C_I for a tension test sepcimen at element 292 ($z=0.85b$) indicated in Fig. 4: (a) $C_I=0.0$ and (b) $C_I=0.001$.

element 292 indicated in Fig. 4 especially near the surface layer. In such a case, it is well known that in the simple shear flow fiber oscillates with a constant period. This behavior depends on the fiber aspect ratio. Especially, for fibers with an infinite aspect ratio, no oscillatory behavior is observed [20]. In Fig. 14(b) it can be seen that the small interaction coefficient C_I of 0.001 has the effect of suppressing the oscillatory behavior.

4.1.3. Dependence on Initial Conditions

To investigate the effect of the initial orientation state at the gate, an aligned orientation state was intentionally introduced at the gate with the same input data as the case of Fig. 5 to 8. Fig. 15 shows the transient fiber orientation states at the grid point 1, center layer, with the aligned initial condition at the gate as injection mold filling proceeds. At the initial stage, fibers around the gate are aligned to be perpendicular to the flow direction due to the strong diverging flow as shown in Fig. 15(a). But, as the melt front advances, fibers near the gate tend to be aligned with the initial orientation as indicated in Fig. 15(b)-(d). This change of orientation of fibers near the gate as melt flow proceeds might be explained as follows: the diverging flow around the gate becomes weaker due to the geometrical effect of the tension test specimen and the convective transport from the gate becomes relatively domiant. It may be noted that fiber orientation away from the gate is not affected by the initial orientation. Also, it should be mentioned that the difference between the case with an aligned initial condition and that with the random initial condition at the gate is observed only at layers close to the center layer. At layers close to the wall, the magnitude of velocity is smaller than the center layer, so the shear flows become dominant compared with the convective transport from the gate. One may recall that the fiber tends to be aligned with the velocity direction when the shear flow is dominant like in the skin layer. In this regard, the difference between the two cases becomes smaller as the layer becomes closer to the wall. One can also observe that the initial orientation state of the melt front has little effect on the final orientation state when the cavity gets filled from the transient fiber orientation states in Fig. 15. Even though the evolution equation for orientation tensor is an initial value problem, the final orientation state depends largely on the velocity gradient fields rather than the initial orientation state.

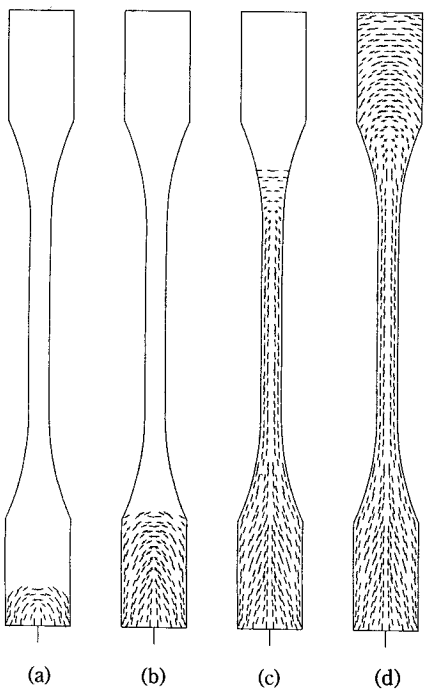

Fig. 15. Transient fiber orientation state at core layer ($z=0$) with the aligned initial condition at the gate: (a) at $t=0.081$ sec, (b) at $t=0.255$ sec, (c) at $t=0.557$ sec and (d) at $t=0.881$ sec.

In the present study it is assumed that fibers remain in a surface parallel to the midsurface while they are moving from the gate to their final positions. However, this assumption is not valid near the melt front region because of the fountain flow effect. Fibers near the melt front region will be deposited to certain layers and subsequently stay at the same layers as the melt front advances. As far as the fiber deposited to a certain layer is concerned, the orientation of the fiber just arriving at the layer should be regarded as an initial orientation with respect to the evolution equation of the orientation tensor. In this regard, as the

initial orientation state of the melt front is found to have little effect on the final orientation state when the cavity gets filled, the final configuration of orientation distribution will show little dependence on the fountain flow effect even if one neglects the fountain flow effecft at the flow front. Of course, it would be much more desirable to take into account the fountain flow effect in the flow simulation and the orientation simulation. However, this will require a lot more complicated analysis and computation time, which is beyond our capability at this moment, and thus the current approach seems to be justifiable.

4.2. Three-Dimensional Example

4.2.1. Podium with a Square Hole

In order to demonstrate the capability of the present work for three-dimensional simulations, chosen is a three-dimensional thin cavity geometry of a podium with a square hole. The dimension of a podium is as follows; maximum width= 10. cm, height=3.0 cm, width of a square hole= 2.0 cm and thickness=0.2 cm. And the input data are as follows; inlet flow rate=50 cm^3/sec, inlet melt temperature=200℃, mold wall temperature =30℃, the number of fibers per unit volume=1/ mm^3, length of fiber=1.0 mm, diameter of fiber= 0.04 mm and phenomenological coefficient C_I= 0.01. Figs. 16 and 17 are numerical simulation results for the filling pattern and fiber orientations, respectively. In Figs. 16 and 17, two graphical results from two different view directions are displayed to show the overall behavior in this three-dimensional cavity geometry. In Fig. 16, it is easily found that the weldline is formed behind the square hole. Fig. 17 shows the fiber orientation state of the three different layers including the core and the skin layer. One should observe the complex orientation state along the weldline behind the obstacle. And the orientation state does not change across the edges since we assumed the preserved orientation state across the folds. This result is favorably compared with Frahan's report [12] in the center layer. It may be noted that Frahan's work has calculated the fiber orientation only at the center layer, as opposed to the present study.

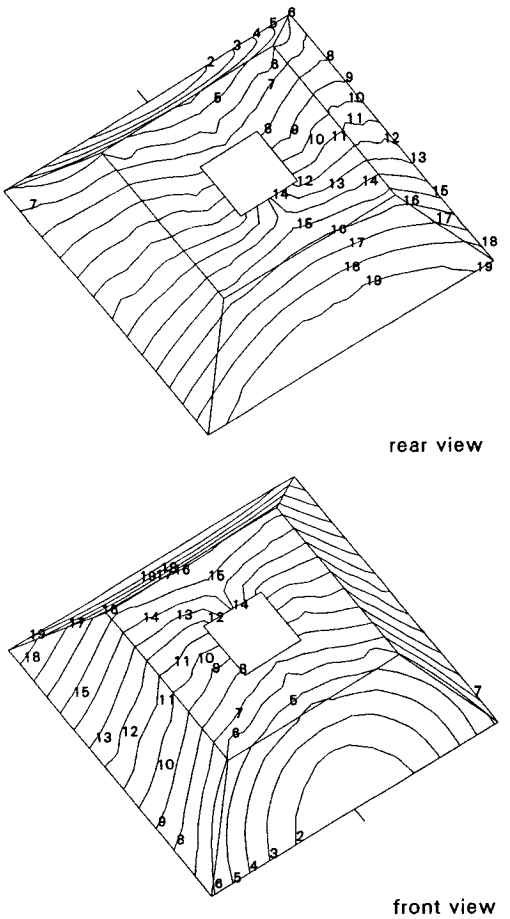

Fig. 16. Filling pattern for a podium with a square hole for constant inlet flow rate, 50 cm^3/sec (step increment=0.031 sec, filling time= 0.59 sec).

5. Conclusions

A numerical simulation method has successfully been developed to predict the three-dimensional fiber orientations of short-fiber-reinforced thermoplastics during the injection molding filling process in three-dimensional mold cavities. The mold filling simulation via a FEM/FDM is based on a new pressure field equation incorporating the additional stress due to presencke of fibers. A compact tensor representation is adopted describing the fiber orientation state at each grid point of

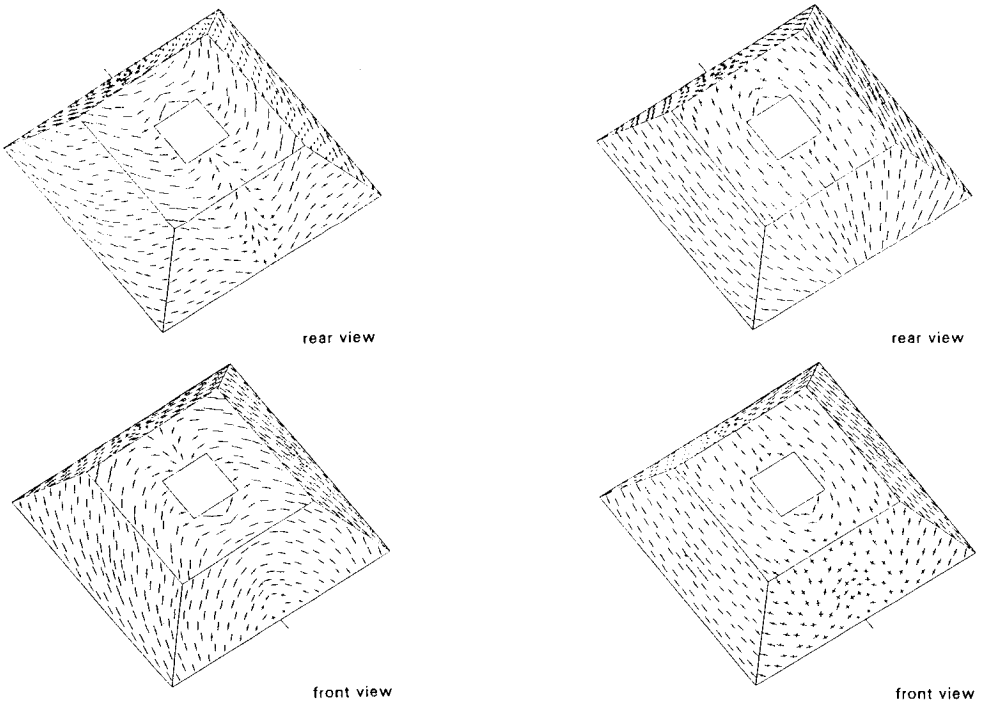

Fig. 17. Fiber orientation state for a podium with a square hole: (a) at 1 layer (z=0), (b) at 2 layer (z=0.27b) and (c) at 7 layer (z=0.96 b).

every element centroid across the thickness of the part. A fourth-order Runge-Kutta method is used to solve the evolution equations of the second-order orientation tensor using an upwinding scheme for the covection terms. The calculation of the orientation tensor is based on the local coordinate system of each element. So, tensor transformation of the orientation tensor is required between the neighboring elements in order to deal with convection terms. Since it is assumed that the fiber orientation state is preserved across the folds, additional tensor transformation is required to evaluate the convection terms when the melt flows across the fold in an arbitrary three-dimensional cavity space. In this way it is possible to predict the transient fiber orientation state in an arbitrary three-dimensional cavity geometry during entire injection mold filling process.

References

1. G.B. Jeffery, *Proc. Roy. Soc.*, **A102**, 161 (1922).
2. R.C. Givler, M.J. Crochet, and R.B. Pipes, *J. Compos. Mater.*, **17**, 330 (1983).
3. F. Folgar and C.L. Tucker, *J. Reinf. Plast. Compos.*, **3**, 98 (1984).
4. S.M. Dinh and R.C. Armstrong, *J. Rheol.*, **28**, 207 (1984).
5. G.K. Batchelor, *J. Fluid Mech.*, **46**, 813 (1971).
6. M.A. Bibbo, S.M. Dinh, and R.C. Armstrong, *J. Rheol.*, **29**, 905 (1985).
7. S.G. Advani and C.L. Tucker, *J. Rheol.*, **31**, 751 (1987).
8. M.C. Altan, S.G. Advani, S.I. Güçeri, and R.B. Pipes, *J. Rheol.*, **33**, 1129 (1989).
9. S.G. Advani and C.L. Tucker, *J. Rheol.*, **34**, 367 (1990).
10. S.G. Advani and C.L. Tucker, *Polym. Compos.*, **11**, 164 (1990).
11. M.C. Altan, S. Subbiah, S.I. Güçeri, and R.B. Pipes, *Polym. Eng. Sci.*, **30**, 848 (1990).
12. H. Henry De Frahan, V. Verleye, F. Dupret, and M.J. Crochet, *Polym. Eng. Sci.*, **32**, 254 (1992).
13. Jin Ko and Jae R. Youn, *The Korean J. of Rheology*, **3**(2), 102 (1991).
14. Seong Jae Lee and Seung Jong Lee, *The Korean J. of Rheology*, **4**(1), 70 (1992).
15. Mi Hye Lee and Ki-Jun Lee, *The Korean J. of Rheology*, **4**(2), 138 (1992).
16. Jin Ko and Jae R. Youn, *The Korean J. of Rheology*, **5**(1), 49 (1993).
17. C.A. Hieber and S.F. Shen, *J. Non-Newt. Fluid Mech.*, **7**, 1 (1980).
18. V.W. Wang, C.A. Hieber, and K.K. Wang, *SPE ANTEC Tech. Papers*, **31**, 826 (1985).
19. C.L. Tucker, *J. Non-Newt. Fluid Mech.*, **39**, 239 (1991).
20. S. Akbar and M.C. Altan, *Polym. Eng. Sci.*, **32**, 810 (1992).